Available online at www.sciencedirect.com
ScienceDirect
Applied Catalysis B: Environmental 80 (2008) 24–31
APPLIED CATALYSIS B: ENVIRONMENTAL
www.elsevier.com/locate/apcatb

# A temperature programmed desorption investigation on the interaction of $Ba_{0.5}Sr_{0.5}Co_{0.8}Fe_{0.2}O_{3-\delta}$ perovskite oxides with $CO_2$ in the absence and presence of $H_2O$ and $O_2$

Aiyu Yan [a,b], Bin Liu [a,b], Yonglai Dong [a], Zhijian Tian [a], Dezheng Wang [c], Mojie Cheng [a,*]

[a] *Dalian Institute of Chemical Physics, Chinese Academy of Sciences, Dalian 116023, China*
[b] *Graduate Schools of the Chinese Academy of Sciences, Beijing 100039, China*
[c] *Department of Chemical Engineering, Tsinghua University, Beijing 100084, China*

Received 21 August 2007; received in revised form 19 October 2007; accepted 6 November 2007
Available online 19 November 2007

## Abstract

The adsorption of $CO_2$ on $Ba_{0.5}Sr_{0.5}Co_{0.8}Fe_{0.2}O_{3-\delta}$ (BSCF) perovskite oxides in the absence and presence of $O_2$ and $H_2O$ at various temperatures was investigated by temperature programmed desorption (TPD). XRD was used to characterize the phase of the samples before and after adsorption. No $CO_2$ desorption peak was observed when $CO_2$ was adsorbed on BSCF at room temperature. A $CO_2$ desorption peak from the decomposition of surface $Sr_{0.6}Ba_{0.4}CO_3$ appeared after $CO_2$ was adsorbed at 400–700 °C. The reactivity of $CO_2$ with BSCF increased with increasing temperature, and the resulted carbonate became more stable. When $CO_2$ and $O_2$ were co-adsorbed, the $CO_2$ desorption peak shifted to lower temperature and the peak area decreased compared with when only $CO_2$ was adsorbed, which was due to the competitive adsorption of $CO_2$ and $O_2$. The adsorption of $CO_2$ on BSCF was promoted in the presence of $H_2O$. A $CO_2$ desorption peak ranging from ca. 250 to 500 °C, assigned to the decomposition of the bicarbonate, was observed when $H_2O$ was added. The amount of $CO_2$ adsorbed on $Ba_{1-x}Sr_xCo_{0.8}Fe_{0.2}O_{3-\delta}$ increased when the barium doping level increased from 0.3 to 1.


*Keywords:* $Ba_{0.5}Sr_{0.5}Co_{0.8}Fe_{0.2}O_{3-\delta}$; Perovskite oxides; Temperature programmed desorption; Carbon dioxide

## 1. Introduction

$Ba_{0.5}Sr_{0.5}Co_{0.8}Fe_{0.2}O_{3-\delta}$ (BSCF) composite oxides have attracted considerable attention as an oxygen separation membrane and solid oxide fuel cell (SOFC) cathode. This material is a mixed ionic and electronic conductor with a cubic perovskite structure. It was first developed as an oxygen permeable membrane material by a 50% substitution of $Sr^{2+}$ in $SrCo_{0.8}Fe_{0.2}O_{3-\delta}$ (SCF) with the larger size cation of $Ba^{2+}$. It has better phase stability and oxygen vacancy diffusivity than SCF [1,2]. Several researchers have reported that $Ba_{0.5}Sr_{0.5}Co_{0.8}Fe_{0.2}O_{3-\delta}$ shows outstanding performance not only as an oxygen permeable membrane [1,3,4] but also when used in membrane reactors for the partial oxidation of methane and ethane to syngas [5–7]. In 2004, Shao and Haile [8] reported the use of BSCF as a low temperature SOFC cathode. They found that the cell had a peak power density as high as 1010 and 402 mW $cm^{-2}$ at 600 and 500 °C, respectively. In addition, BSCF has good compatibility with electrolytes such as $Sm_2O_3$ doped $CeO_2$ (SDC) [8,9] and $La_{1-x}Sr_xGa_{1-y}Mg_yO_3$ (LSGM) [10] which have desirable ionic conductivity at intermediate and low temperatures. Mat et al. [11] reported that BSCF was also suitable for the cathode materials for the ceria–carbonate composite electrolytes to be used in direct alcohol fuel SOFC at 300–600 °C. Therefore, BSCF is regarded as one of the most promising cathodes for the low temperature SOFC.

However, the instability of the perovskite containing alkaline-earth elements in the presence of $CO_2$ and $H_2O$ emerged as one of the limiting factors for their application. For example, Yi et al. [12] reported that $Sr_{0.95}Co_{0.8}Fe_{0.2}O_{3-\delta}$ membrane was partially decomposed when an air stream containing both $CO_2$ and $H_2O$ was used as the feed gas. Similar results were also found by Pei et al. [13] after they employed a $Sr(Co_{1-x}Fe_x)O_{3-\delta}$ hollow fiber membrane for the partial

* Corresponding author. Tel.: +86 411 84379049; fax: +86 411 84379049.
*E-mail address:* mjcheng@dicp.ac.cn (M. Cheng).

0926-3373/$ – see front matter 
doi:10.1016/j.apcatb.2007.11.007

oxidation of methane. Carolan et al. [14] described that the oxygen permeation flux of $La_{0.8}Ba_{0.2}Co_{0.8}Fe_{0.2}O_{3-\delta}$ decreased significantly when 430 ppm $CO_2$ was introduced into the feed gas. Zakowsky et al. [15] discovered that $BaCe_{0.9}Y_{0.1}O_{3-\delta}$ can be converted to the carbonate, accompanied by disruption of the perovskite, in pure $CO_2$ at 850–1000 °C. Even at 750 °C, $BaCe_{0.9}Y_{0.1}O_{3-\delta}$ tended to convert to the carbonate when the $CO_2$ content was higher than 9%. Very recently, Arnold et al. [16] published results concerning the influence of $CO_2$ on the oxygen permeation performance and the microstructure of perovskite-type $(Ba_{0.5}Sr_{0.5})(Co_{0.8}Fe_{0.2})O_{3-\delta}$ membranes. They found that using pure $CO_2$ as the sweep gas at 875 °C caused an immediate stop of the oxygen permeation flux which, however, could be recovered by sweeping with pure helium. Examination of the microstructure clearly indicated the decomposition of the perovskite structure up to a depth of 40–50 μm when it was exposed to $CO_2$ for more than 4300 min. Previously, we had already pointed out that the BSCF cathode was susceptible to $CO_2$ attack at 450–750 °C. A decrease of the cell performance and increase of the polarization resistance were observed when $CO_2$ was supplied to the cathode gas line [17]. A detailed surface analysis of the BSCF cathode after operation in 1% $CO_2/O_2$ at 450 °C for 24 h revealed that the cathode surface was destroyed and the carbonates of Sr and Ba were formed on the top of the cathode layer [18]. Therefore, it is important to understand the interaction of BSCF with $CO_2$, $O_2$ and $H_2O$ taking into account that BSCF is considered as a highly promising cathode material for solid oxide fuel cells and oxygen separation membrane. Temperature programmed desorption (TPD) is a sensitive technique for the characterization of the interaction between adsorbed molecules and solid surfaces [19–21]. In the present work, the behavior of $CO_2$ over $Ba_{0.5}Sr_{0.5}Co_{0.8}Fe_{0.2}O_{3-\delta}$ perovskite oxides at various temperatures both in the absence and presence of $O_2$ and $H_2O$ was investigated by the TPD technique.

## 2. Experimental

The $Ba_{0.5}Sr_{0.5}Co_{0.8}Fe_{0.2}O_{3-\delta}$ powder was prepared by the combined citrate and EDTA complexing method previously described [17]. The TPD analysis was performed using 100.0 mg catalyst placed in a fixed-bed U-shaped quartz reactor. The samples were first pretreated in air at 500 °C for 60 min and then flushed with a $CO_2$/He (1%, 70 ml min$^{-1}$) or $CO_2$/He (1%, 50 ml min$^{-1}$) and $O_2$/He (5%, 50 ml min$^{-1}$) gas mixture for 2 h at various temperatures. The sample was subsequently cooled down to room temperature under the same atmosphere, followed by heating up to 950 °C at a constant heating rate of 10 °C min$^{-1}$ in He stream gas. In order to study the chemical stability of BSCF in the presence of both $CO_2$ and $H_2O$, $CO_2$/He (1%, 50 ml min$^{-1}$) was passed through a saturator at room temperature where the gas was saturated by $H_2O$ and mixed with 5% $O_2$/He (50 ml min$^{-1}$) before its introduction into the reactor. The effluent gas was analyzed by a mass spectrometer (MS, Ominstar Balzers). The MS intensities for $CO_2$ (44), $O_2$ (32) and $H_2O$ (18) were recorded as a function of temperature.

The TPD results were simulated using a plug flow reactor model and the kinetics expression shown as (1):

$$r_i = A_i C_i^n \exp\left(\frac{-E_{\mathrm{di}}}{RT}\right),\qquad \frac{\partial C_i}{\partial t} + \frac{\partial (VC_i)}{\partial x} = \sum_j r_j \tag{1}$$

where $C_i$ is the concentration of adsorbed species on BSCF active sites, $A_i$ is the preexponential factor, $E_{\mathrm{di}}$ is the activation energy, $n$ is the reaction order, and $V$ is the superficial flow velocity. The reactor equations were integrated numerically using a first order upwind scheme algorithm for solving partial differential equations for a given set of parameters [22]. The fit of the simulated TPD peak to experimental results to determine the optimized kinetic parameters was performed by the use of the visual inspection of the computed and experimental curves to judge which was the best-fit computed curve. This was chosen in preference to the use of the sum of least squares and proportional weighting (some other weightings that were also examined) as the best-fit criterion because this latter criterion gave a poorer fit.

In order to determine the crystal structure of the as-prepared BSCF powder and the powder after pretreatment in 1% $CO_2$/He gas mixture at various temperatures, XRD was conducted on a RigakuD/max-2500PC X-ray diffractometer using Cu $K_\alpha$ radiation (λ = 1.54108 Å) in $2\theta$ ranging from 15° to 80°.

## 3. Results and discussion

### 3.1. Adsorption of $CO_2$ on BSCF at various temperatures

Fig. 1(a) shows the $CO_2$-TPD profiles of the BSCF powder after pretreatment in 1% $CO_2$/He for 2 h at various temperatures. There was no $CO_2$ desorption peak when $CO_2$ was adsorbed at room temperature. For the sample pretreated at 400 °C, the desorption of $CO_2$ started from 424 °C and reached a peak at 674.7 °C. With the increase of the adsorption temperature to 500, 600 and 700 °C, the $CO_2$ desorption peak gradually shifted to 714, 788 and 809 °C, respectively, implying that the adsorption of $CO_2$ on BSCF would be possibly strengthened with increasing temperature. In addition, a shoulder peak at 627 °C appeared in the profile of the sample pretreated at 500 °C. The peak area, which represented the amount of $CO_2$ adsorbed, increased when the adsorption temperature was increased from 400 to 700 °C. This result suggested that reaction between $CO_2$ and BSCF became more serious at high temperatures. According to the variance of peak maximum temperature ($T_p$) and the desorption peak area of $CO_2$, it can be concluded that the reactivity of $CO_2$ with the BSCF surface increased with increasing temperatures.

The TPD profiles were deconvoluted by the kinetics expression (1) using the method described in Section 2, and the corresponding kinetic parameters are summarized in Table 1. The best fit of Eq. (1) to the experimental results of the sample pretreated at 400 °C was obtained by using the first order desorption reaction and a desorption activation energy of

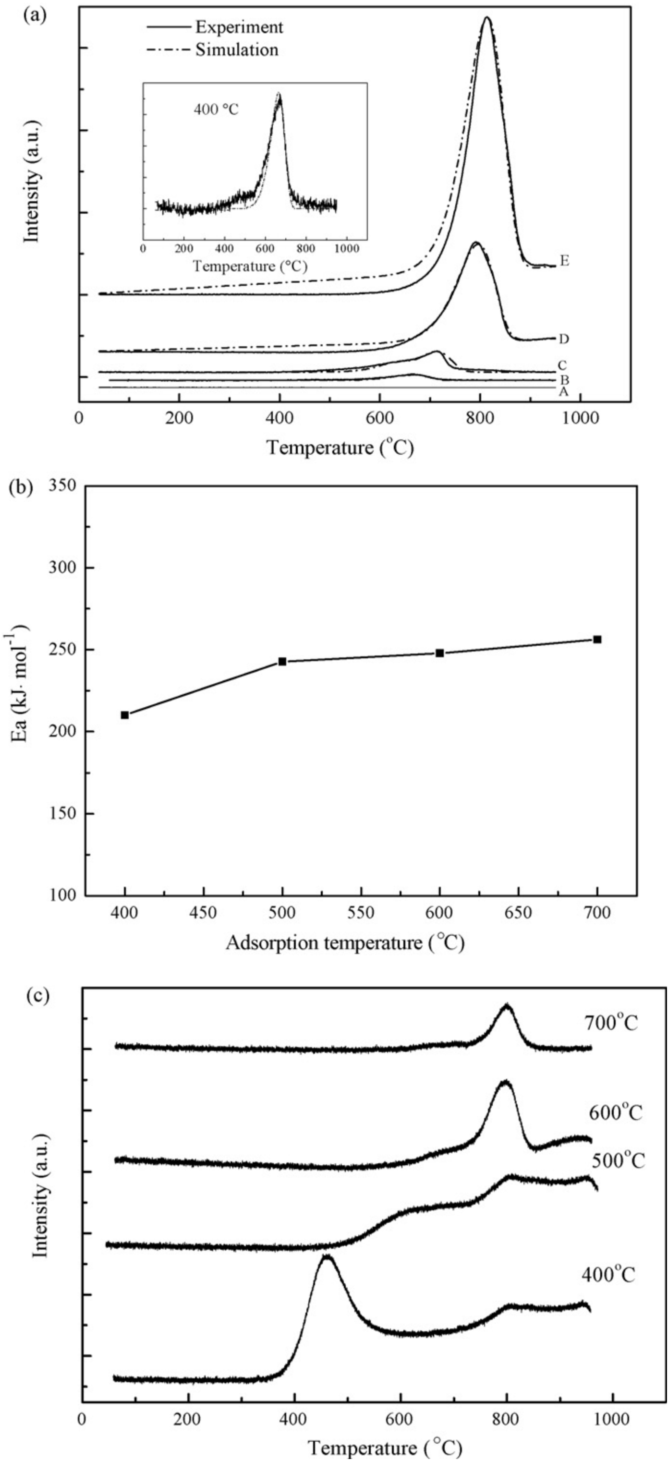


Fig. 1. (a) $CO_2$-TPD profiles from BSCF after $CO_2$ adsorption at different temperatures for 2 h, and simulated TPD profiles showing the deconvolution of the peaks. (A) Room temperature, (B) 400 °C, (C) 500 °C, (D) 600 °C and (E) 700 °C. (b) The desorption activation energy as a function of adsorption temperature. (c) $O_2$-TPD from BSCF after $CO_2$ adsorption for 2 h at various temperatures.

210 kJ mol$^{-1}$. A first order kinetics expression was used for desorption because a parameter estimation using a second order desorption kinetics expression gave a much poorer fit. Deconvolution of the profile of the sample pretreated at

Table 1
Parameters estimated from the TPD profiles in Fig. 1

| | $E$ (kJ mol$^{-1}$) | $A$ (min$^{-1}$) | $n$ |
|---|---|---|---|
| 400 °C | 210 | $1.8 \times 10^8$ | 1.0 |
| 500 °C | 210 | $9 \times 10^8$ | 1.0 |
| | 243 | $7 \times 10^8$ | 1.0 |
| 600 °C | 248 | $3 \times 10^8$ | 1.0 |
| 700 °C | 256 | $4.8 \times 10^8$ | 1.0 |

500 °C yielded two peaks with activation energies of 210 and 243 kJ mol$^{-1}$. For the samples pretreated at 600 and 700 °C, the activation energies were 248 and 256 kJ mol$^{-1}$, respectively. The desorption activation energy was an important kinetic parameter which reflected how strongly the adsorbate was bonded with the surface of adsorbent. Obviously, the adsorption temperature affected the interaction of $CO_2$ with BSCF. In order to clarify this point, the desorption activation energy as a function of adsorption temperature was presented in Fig. 1(b). It can be seen that the desorption activation energy increased with the adsorption temperature. Especially from 500 to 700 °C, a quasi-linear increase of the desorption activation energy with the increase of adsorption temperature was found. Generally speaking, the higher the desorption activation energy was, the stronger was the adsorbate bonded with the adsorbent [23,24]. The above results confirmed that increasing temperature could enhance the interaction of $CO_2$ with BSCF.

The thermodynamics of the system is such that both barium and strontium oxides will react with $CO_2$. It was reported that particles of $SrCO_3$, $BaCO_3$ or double salts of $Sr_xBa_{1-x}CO_3$ can be decomposed at 600–900 °C [25–28]. In the previous work, XPS and EDX analysis of a BSCF cathode operated in 1% $CO_2$/$O_2$ at 450 °C showed that a carbonate layer enriched with strontium was formed on the top of the cathode surface [18]. The enrichment with strontium was probably because the mixing enthalpy of $(Ba_xSr_{1-x})CO_3$ solid solutions reached a maximum at $x = 0.35$ [29]. Based on these reports, we assigned the $CO_2$ desorption peak to the decomposition of the surface carbonates of Ba and/or Sr. In order to identify the composition of the carbonates, XRD measurements of these samples were conducted. The XRD results clearly indicated the formation of $Sr_{0.6}Ba_{0.4}CO_3$, which is discussed below. Criado et al. [25] investigated the decomposition of $Ba_xSr_{1-x}CO_3$ by analyzing the CRTA (constant rate thermal analysis) and TG curves of the sample under high vacuum, and reported that the activation energy for $Sr_{0.6}Ba_{0.4}CO_3$ decomposition was 247 kJ mol$^{-1}$. This value is very close to our data from the samples pretreated at 500, 600 and 700 °C. The relatively low activation energy for the sample treated at 400 °C is probably due to the highly dispersed nature and small amount of the carbonate on the surface.

$O_2$-TPD profiles can provide effective information on the behavior of lattice oxygen in composite oxide materials. Fig. 1(c) shows the $O_2$-TPD profiles of the samples after $CO_2$ adsorption at various temperatures. The $O_2$-TPD profile of the sample after $CO_2$ adsorption at 400 °C comprised two $O_2$ desorption peaks. One was at around 450 °C and was related to

the reduction of $Co^{4+}$ and/or $Fe^{4+}$ to $Co^{3+}$ and/or $Fe^{3+}$, and the other peak was at around 800 °C corresponding to the reduction of $Co^{3+}$ to $Co^{2+}$ [1]. For the sample pretreated at 500 °C, the first peak stared from 470 °C and centered at 630 °C. The intensity of this peak was much weaker than that of the sample treated at 400 °C. When the adsorption peak was increased to 600 and 700 °C, the first peak completely disappeared. The $T_p$ of the high temperature peak in all the profiles appeared at around 800 °C. But the intensity was much stronger for the sample treated at 600 and 700 °C than that treated at 400 and 500 °C. Oxygen vacancies can be formed when BSCF is treated in $CO_2$/He at high temperatures due to the extremely low oxygen partial pressure [30]. In order to keep the neutrality condition of the material, part of $Co^{4+}$ and $Fe^{4+}$ ions transferred to $Co^{3+}$ and $Fe^{3+}$ ions, which explained the disappearance of the low temperature peak and the increase of the intensity of the high temperature peak when the sample was treated at 600 and 700 °C. Nomura et al. [31] have pointed out that oxygen vacancies in the perovskite structure can contribute to the formation of the carbonate. They proposed that perovskite oxides with lattice vacancies produced at high temperature easily adsorbed $CO_2$. The higher the temperature at which the samples were pretreated, the more were the oxygen vacancies generated, which may be one reason why $CO_2$ reacted with BSCF easily at high temperatures.

The XRD patterns of the samples are shown in Fig. 2. The fresh BSCF powder showed the typical perovskite structure. After treatment in 1% $CO_2$/He, the materials still had the perovskite structure. However, the diffraction peaks of $Sr_{0.6}Ba_{0.4}CO_3$ were observed after pretreatment at 700 °C [16]. A weak diffraction peak at 28°, which can be assigned to BaO, also appeared. For the samples treated at 400–600 °C, only the strongest double peaks of $Sr_{0.6}Ba_{0.4}CO_3$ at 24.5° and 25.1° could be observed. The intensity of this peak became weaker with decreasing treatment temperature, which agreed well with the TPD results. With increased adsorption temperature, the amount of carbonate increased. In addition, the carbonates can grow into larger particles at higher temperatures.

### 3.2. Co-adsorption of $CO_2$ and $O_2$ on BSCF at various temperatures

Fig. 3 shows the $CO_2$-TPD profiles from the BSCF powder after $CO_2$/He–$O_2$/He co-adsorption for 2 h at 400–700 °C. It can be seen that $T_p$ of $CO_2$ desorption peak shifted to higher values and the area of the peak increased gradually when the adsorption temperature was increased from 400 to 600 °C. The respective $T_p$ were 653, 666 and 733 °C when $CO_2$ was adsorbed at 400, 500 and 600 °C. However, for the sample pretreated at 700 °C, $T_p$ was at 714 °C, which was slightly lower than that of the sample treated at 600 °C, and the area of the $CO_2$ desorption peak was very close to that of the sample treated at 400 °C. It was found that the surface carbonate decomposed at lower temperatures when compared with the case when only $CO_2$ was adsorbed. The area of the desorption peak for $CO_2$ adsorption in the presence of $O_2$ decreased by 29%, 48%, 69% and 97% for adsorption temperatures of 400, 500, 600 and 700 °C, respectively, compared with the case of $CO_2$ adsorption without $O_2$. It is clear that $O_2$ also can adsorb on the surface of BSCF and even get incorporated into its bulk. Therefore, $CO_2$ and $O_2$ were competitively adsorbed on the BSCF surface. In addition, the existence of $O_2$ can maintain oxygen releasing and adsorbing of oxygen at a quasi-state and thus reduce the number of oxygen vacancies in the bulk and on the surface. On the one hand, the adsorption of $CO_2$ leads to the formation of the surface carbonate, and on the other hand, the adsorption of $O_2$ helps to stabilize the perovskite structure. From the TPD results in Figs. 1–3, it can be deduced that the inhabiting effect of $O_2$ on $CO_2$ adsorption also increased with temperature. At 700 °C, the adsorption of $O_2$ was the dominant reaction on the BSCF surface. These results are in good agreement with the measurement of the cell performance in the presence of $CO_2$

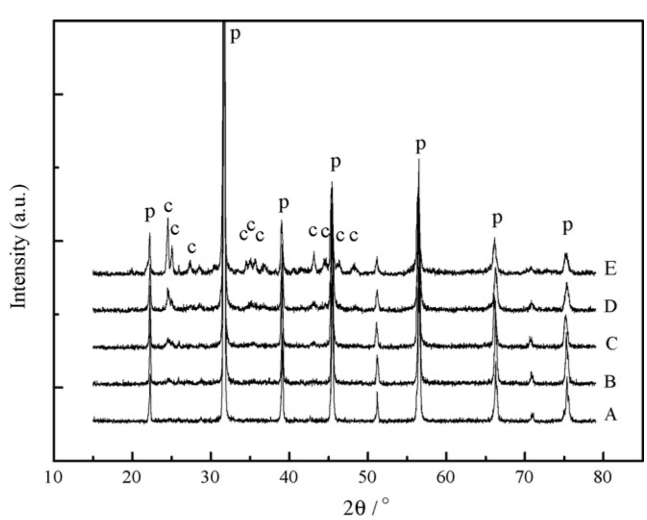


Fig. 2. XRD patterns of (A) fresh BSCF and BSCF after $CO_2$ adsorption for 2 h at (B) 400 °C, (C) 500 °C, (D) 600 °C and (E) 700 °C. p: perovskite, and c: $Sr_{0.6}Ba_{0.4}CO_3$.

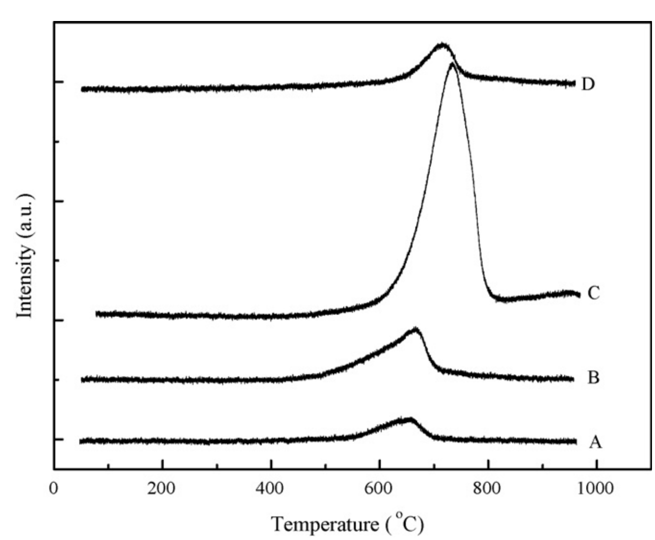


Fig. 3. $CO_2$-TPD profiles from BSCF after $CO_2$–$O_2$ co-adsorption at (A) 400 °C, (B) 500 °C, (C) 600 °C and (D) 700 °C for 2 h.

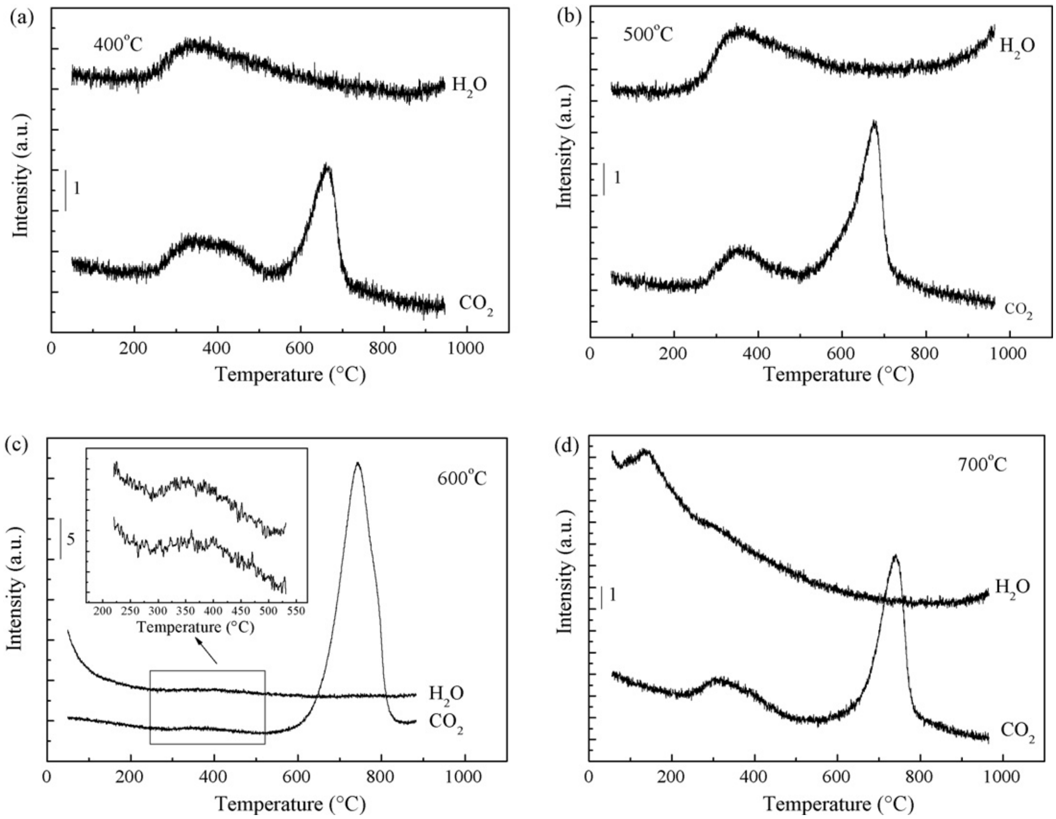


Fig. 4. $CO_2$-TPD and $H_2O$-TPD profile from BSCF after $CO_2$–$O_2$ co-adsorption in the presence of $H_2O$ at (a) 400 °C, (b) 500 °C, (c) 600 °C and (d) 700 °C for 2 h.

in a previous investigation [17]. It was found that the $CO_2$ poisoning effect on the cell performance ($CO_2/O_2$ as oxidant) was less severe when the operation temperature was increased from 600 to 700 °C. Recently, Arnold et al. [16] also reported the competitive adsorption of $CO_2$ and $O_2$. They observed a strong acceleration of the performance degradation if the $CO_2$ concentration in the feed air of the BSCF membrane increased.

### *3.3. Co-adsorption of $CO_2$ and $O_2$ in presence of $H_2O$ on BSCF at various temperatures*

Fig. 4 shows the $CO_2$ and $H_2O$ TPD profiles from BSCF after $CO_2$–$O_2$ was co-adsorbed in the presence of $H_2O$ at different temperatures. The main $CO_2$ desorption peak appeared at 663, 675, 742 and 741 °C after $CO_2$–$H_2O$ was adsorbed at 400, 500, 600 and 700 °C, respectively. It can be seen that $T_p$ of the main peak is slightly higher than that in Fig. 3, and the peak areas are also larger at the same time. In addition, a broad peak from ca. 250 to 500 °C, which was almost independent of the adsorption temperature, was observed in all the profiles shown in Fig. 4. It is interesting to note that a broad band of $H_2O$ desorption can be seen at almost the same temperature range of the $CO_2$ peak at low temperature. Both theoretical and experimental studies have indicated that a $H_2O$–$CO_2$ van der Waals complex is formed when both $CO_2$ and $H_2O$ are present in the gas phase [32,33]. The formation of bicarbonates over $TiO_2$ oxide has been widely reported and it was suggested that oxygen vacancies played an essential role in the formation of the bicarbonates [34–36]. For instance, Herderson [36] described the formation of a bicarbonate when $TiO_2$ (1 1 0) was exposed to $H_2O$–$CO_2$ simultaneously. However, there was no evidence for bicarbonate formation if the vacancy sites were filled with OH groups prior to $H_2O$–$CO_2$ exposure. Yi et al. [12] found that a bicarbonate was also likely to form on a $Sr_{0.95}Co_{0.8}Fe_{0.2}O_{3-\delta}$ membrane surface if the feed gas contained $H_2O$–$CO_2$ impurities. Here, it is reasonable to assign the low desorption peak of $CO_2$ to the decomposition of bicarbonates due to the simultaneous desorption of $H_2O$ and $CO_2$.

Fig. 5 compares the $O_2$-TPD spectra of the samples after the co-adsorption of $CO_2$–$O_2$ and $CO_2$–$O_2$–$H_2O$. Due to the presence of $O_2$, the $O_2$-TPD profiles after the co-adsorption of $CO_2$–$O_2$ consisted of two $O_2$ desorption peaks. One was a strong peak locating from ca. 300 to 620 °C, and the other one was a weak peak with $T_p$ at 800 °C. After co-adsorption of $CO_2$–$O_2$–$H_2O$, the start of the first $O_2$ releasing peak shifted to a higher temperature and the intensity decreased markedly as compared with the former case, indicating that a much larger amount of lattice oxygen was released during $CO_2$–$O_2$–$H_2O$ co-adsorption. Although the mechanism of $CO_2$–$O_2$–$H_2O$ adsorption on BSCF is not clear, it can be concluded that more oxygen vacancies were present during the process. It has been reported that water could incorporate into the perovskite materials such as $(Ba_{1-x}La_x)_2In_2O_{5+x}\square_{1-x}$ [37], $SrTiO_3$, $SrZrO_3$ [38] and $La(Co, Mn, Fe)_{1-x}(Cu, Pd)_xO_3$ [39] by occupying the oxygen vacancies due to the formation of H-bonds between the water hydrogen and surface oxygen as well as the water molecules themselves. Recently, Lindholm et al. [40] reported that the storage performance of Pt/Ba/Al catalysts for $NO_x$ was

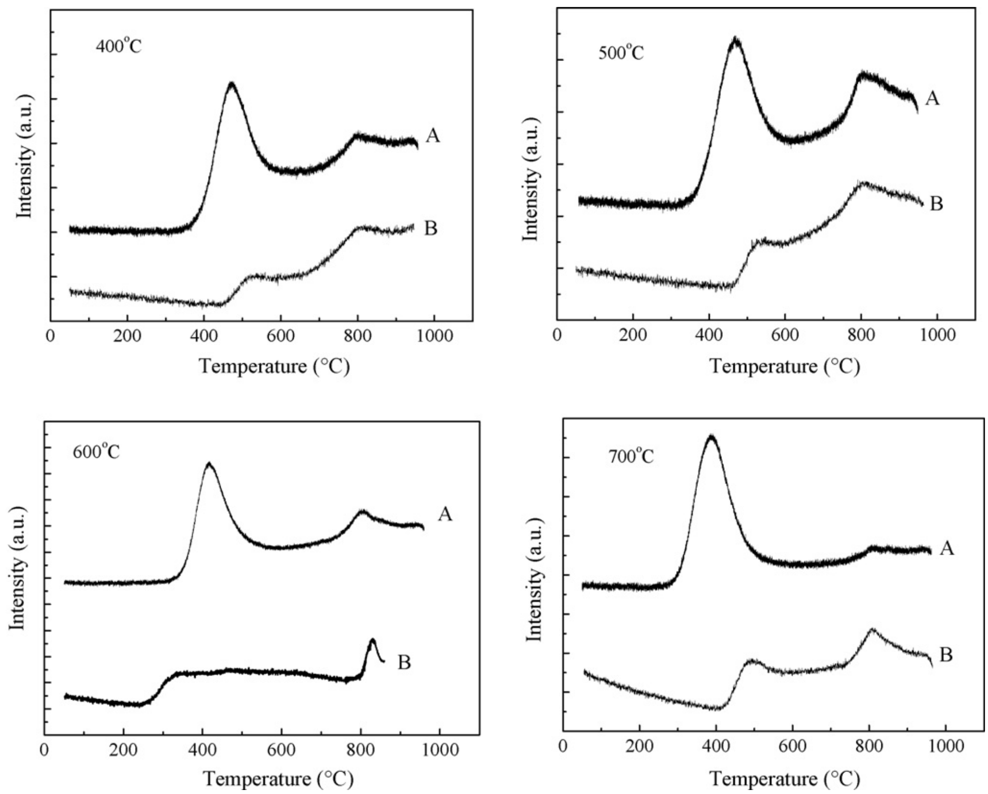


Fig. 5. Comparison of $O_2$-TPD profiles from BSCF after $CO_2$–$O_2$ co-adsorption in the absence and presence of $H_2O$. (A) Co-adsorption of $CO_2$–$O_2$ and (B) co-adsorption of $CO_2$–$O_2$ in the presence of $H_2O$.

decreased in the presence of $H_2O$ and $CO_2$ due to the formation of hydroxides and carbonates. Grillo et al. [41] also found that the formation of carbonates species was more evident in steam conditions than that in dry conditions when using $Co_3O_4$ catalyst for CO oxidation. Probably, the presence of both $H_2O$ and $CO_2$ could inhibit the adsorption of $O_2$, resulting in the increase of oxygen vacancies and more serious poisoning effect.

Fig. 6 compares the area of the $CO_2$ desorption peak after the samples were pretreated under different conditions. It was found that the desorption area decreased following the order: $CO_2 > CO_2–O_2–H_2O > CO_2–O_2$. This result confirmed that $H_2O$ can aggravate the poisoning effect of $CO_2$ while the presence of $O_2$ helped to stabilize the perovskite structure.

### 3.4. Adsorption of $CO_2$ on $Ba_xSr_{1-x}Co_{0.8}Fe_{0.2}O_{3-\delta}$ at 600 °C

Figs. 7 and 8 show the TPD spectra and the corresponding XRD patterns of $Ba_xSr_{1-x}Co_{0.8}Fe_{0.2}O_{3-\delta}$ $(0 \leq x \leq 1))$ after $CO_2$ adsorption for 2 h at 600 °C. The profile of $SrCo_{0.8}Fe_{0.2}O_{3-\delta}$ showed two peaks at 745 and 803 °C. The corresponding XRD pattern identified the formation of $SrCO_3$. Scholten et al. [42] also described that the TG-DTA curve of $SrCO_3$ consisted of two peaks, which was probably due to the increase of the $CO_2$ partial pressure during the desorption process. In addition, the XRD pattern of $SrCo_{0.8}Fe_{0.2}O_{3-\delta}$ revealed that this material had changed to brownmillerite-type structure, $Sr_2Co_{1.6}Fe_{0.4}O_5$, due to its instability below 1073 K at $P_{O_2}$ lower than around 0.1 atm.

The temperature of the $CO_2$ desorption peak shifted to 762, 808 and 841 °C with $x = 0.3$, 0.7 and 1. The area of the peak increased when the barium doping level increased from 0.3 to 1. The diffractions at 24.1°, 24.4°, 31.1–31.9°, 42.5° on the XRD patterns of $BaCo_{0.8}Fe_{0.2}O_{3-\delta}$ and $Ba_{0.7}Sr_{0.3}Co_{0.8}Fe_{0.2}O_{3-\delta}$ indicated the formation of $BaCO_3$. From the thermodynamics, $BaCO_3$ is more stable than $SrCO_3$ and decomposes at a higher temperature [42,43]. The diffraction at ca. 27°, which can be assigned to $BaCoO_2$, suggested the disruption of the perovskite.

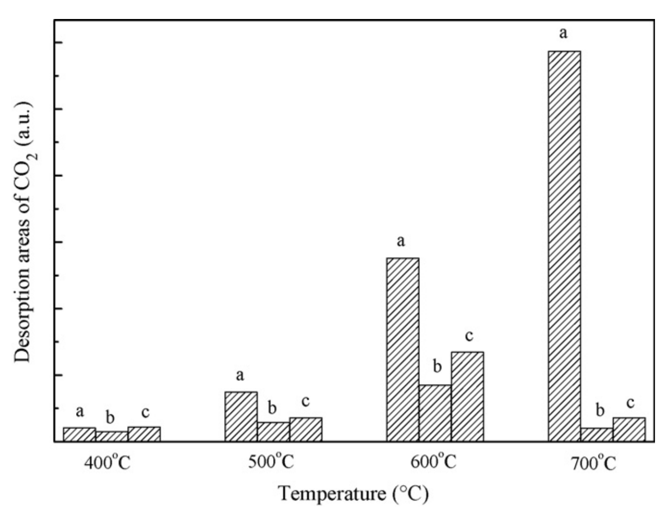


Fig. 6. Variation in the desorption areas of $CO_2$ under various conditions. (a) $CO_2$ adsorption alone, (b) $CO_2$–$O_2$ co-adsorption and (c) $CO_2$–$O_2$–$H_2O$ co-adsorption.

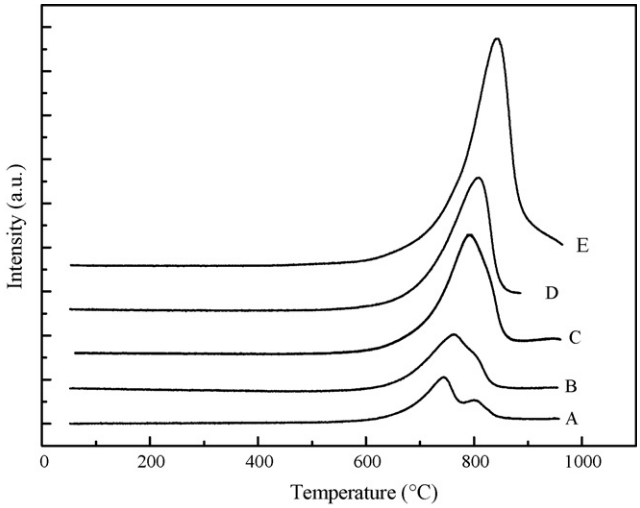


Fig. 7. $CO_2$-TPD profile from $Ba_xSr_{1-x}Co_{0.8}Fe_{0.2}O_{3-\delta}$ after $CO_2$ adsorption at 600 °C for 2 h. (A) $SrCo_{0.8}Fe_{0.2}O_{3-\delta}$, (B) $Ba_{0.3}Sr_{0.7}Co_{0.8}Fe_{0.2}O_{3-\delta}$, (C) $Ba_{0.5}Sr_{0.5}Co_{0.8}Fe_{0.2}O_{3-\delta}$, (D) $Ba_{0.7}Sr_{0.3}Co_{0.8}Fe_{0.2}O_{3-\delta}$ and (E) $BaCo_{0.8}Fe_{0.2}O_{3-\delta}$.

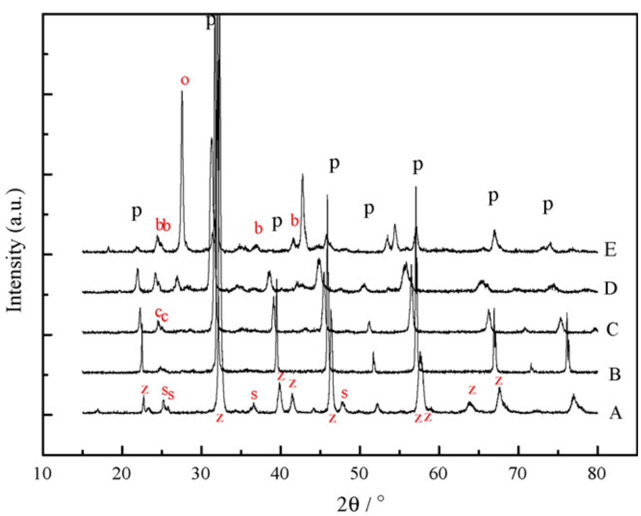


Fig. 8. XRD patterns of $Ba_xSr_{1-x}Co_{0.8}Fe_{0.2}O_{3-\delta}$ after $CO_2$ adsorption at 600 °C for 2 h. (A) $SrCo_{0.8}Fe_{0.2}O_{3-\delta}$, (B) $Ba_{0.3}Sr_{0.7}Co_{0.8}Fe_{0.2}O_{3-\delta}$, (C) $Ba_{0.5}Sr_{0.5}Co_{0.8}Fe_{0.2}O_{3-\delta}$, (D) $Ba_{0.7}Sr_{0.3}Co_{0.8}Fe_{0.2}O_{3-\delta}$ and (E) $BaCo_{0.8}Fe_{0.2}O_{3-\delta}$. p: perovskite, c: $Sr_{0.6}Ba_{0.4}CO_3$, s: $SrCO_3$, b: $BaCO_3$, z: brownmillerite, and o: $BaCoO_2$.

As for $Ba_{0.7}Sr_{0.3}Co_{0.8}Fe_{0.2}O_{3-\delta}$, only weak diffraction peaks at 24.9° and 25.3° associated with the carbonate was observed. The TPD and XRD results suggested that $BaCo_{0.8}Fe_{0.2}O_{3-\delta}$ and $Ba_{0.7}Sr_{0.3}Co_{0.8}Fe_{0.2}O_{3-\delta}$ were more susceptible to $CO_2$ attack compared with the samples with other compositions.

## 4. Conclusion

The interaction between $CO_2$ and $Ba_{0.5}Sr_{0.5}Co_{0.8}Fe_{0.2}O_{3-\delta}$ composite oxides was investigated by TPD both in the presence and absence of $O_2$ and $H_2O$. $CO_2$ can adsorb on and react with BSCF from 400 to 700 °C to form $Sr_{0.6}Ba_{0.4}CO_3$. In the case of $CO_2$ adsorption without $O_2$, the reactivity of $CO_2$ over BSCF surface increased with increasing temperature. $CO_2$ and $O_2$ were competitively adsorbed on BSCF. At 700 °C, adsorption of $O_2$ was the dominant reaction on the BSCF surface. The presence of $H_2O$ aggravated the $CO_2$ poisoning effect, which was probably the result of the formation of the bicarbonate. The amount of $CO_2$ adsorbed on $Ba_{1-x}Sr_xCo_{0.8}Fe_{0.2}O_{3-\delta}$ increased when the barium doping level increased from 0.3 to 1.

## Acknowledgements

The authors gratefully acknowledge financial supports from the Ministry of Science and Technology of China (Grant nos. 2004CB719506, 2005CB221404 and 2006AA05z147), National Natural Science Foundation of China (Grant no. 20676132) and European Committee (SOFC 600).

## References


[1] Z. Shao, W. Yang, Y. Cong, H. Dong, J. Tong, G. Xiong, J. Membr. Sci. 172 (2000) 177–188.
[2] H. Wang, Y. Cong, W. Yang, J. Membr. Sci. 210 (2002) 259–271.
[3] H. Wang, R. Wang, D.T. Liang, W. Yang, J. Membr. Sci. 243 (2004) 405–415.
[4] P. Zeng, Z. Chen, W. Zhou, H. Gu, Z. Shao, S. Liu, J. Membr. Sci. 291 (2007) 148–156.
[5] Z. Shao, G. Xiong, H. Dong, W. Yang, L. Lin, Sep. Purif. Technol. 25 (2001) 97–116.
[6] H. Wang, Y. Cong, W. Yang, Catal. Today 82 (2003) 157–166.
[7] H. Wang, Y. Cong, W. Yang, J. Membr. Sci. 209 (2002) 143–152.
[8] Z. Shao, S.M. Haile, Nature 431 (2004) 170–173.
[9] Z. Duan, A. Yan, Y. Dong, C. You, M. Cheng, W. Yang, Chin. J. Catal. 26 (2005) 1–3.
[10] J. Peña-Martínez, D. Marrero-López, J.C. Ruiz-Morales, B.E. Buergler, P. Nùñez, L.J. Gauckler, J. Power Sources 159 (2006) 914–921.
[11] M.D. Mat, X. Liu, Z. Zhu, B. Zhu, Int. J. Hydrogen Energy 32 (2007) 796–801.
[12] J. Yi, S. Feng, Y. Zuo, W. Liu, C. Chen, Chem. Mater. 17 (2005) 5856–5861.
[13] S. Pei, M.S. Kleefisch, T.P. Kobylinski, J. Faber, C.A. Udovich, V. Zhang-McCoy, B. Dabrowski, U. Balachandran, R.L. Mieville, R.B. Poeppel, Catal. Lett. 30 (1995) 201–212.
[14] M.F. Carolan, P.N. Dyer, J.M. LaBar, R.M. Thorogood, US Patent 5,240,473 (1993).
[15] N. Zakowsky, S. Williamson, J.T.S. Irvine, Solid State Ionics 176 (2005) 3019–3026.
[16] M. Arnold, H. Wang, A. Feldhoff, J. Membr. Sci. 293 (2007) 44–52.
[17] A. Yan, M. Cheng, Y. Dong, W. Yang, V. Maragou, S. Song, P. Tsiakaras, Appl. Catal. B 66 (2006) 64–71.
[18] A. Yan, V. Maragou, A. Arico, M. Cheng, P. Tsiakaras, Appl. Catal. B 76 (2007) 320–327.
[19] A. Kotsifa, D.I. Kondarides, X.E. Verykios, Appl. Catal. B 72 (2007) 136–148.
[20] T. Nobukawa, K. Sugawara, K. Okumura, K. Tomishige, K. Kunimori, Appl. Catal. B 70 (2007) 342–352.
[21] G. Piazzesi, O. Kröcher, M. Elsener, A. Wokaun, Appl. Catal. B 65 (2006) 55–61.
[22] W.F. Ames, Numerical Methods for Partial Differential Equations, third ed., Academic Press, New York, 1992.
[23] H. Xi, Z. Li, H. Zhang, X. Li, X. Hu, Sep. Purif. Technol. 31 (2003) 41–45.
[24] M. Yu, Z. Li, Q. Xia, H. Xi, S. Wang, Chem. Eng. J. 132 (2007) 233–239.
[25] J.M. Criado, M.J. Dianez, M. Macias, Thermochim. Acta 171 (1990) 229–238.
[26] F. Rohr, S.D. Peter, E. Lox, M. Kögel, A. Sassi, L. Juste, C. Rigaudeau, G. Belot, P. Gēlin, M. Primet, Appl. Catal. B 70 (2007) 189–197.
[27] J. Rynkowski, P. Samulkiewicz, A.K. Ladavos, P.J. Pomonis, Appl. Catal. A 263 (2004) 1–9.

[28] K.H. Ryu, S.M. Haile, Solid State Ionics 125 (1999) 355–367.
[29] I.A. Kiseleva, A.R. Kotelnikov, K.V. Martynov, L.P. Ogorodova, Ju.K. Kabalov, Phys. Chem. Miner. 21 (1994) 392–400.
[30] Z. Shao, G. Xiong, J. Tong, H. Dong, W. Yang, Sep. Purif. Technol. 25 (2001) 419–429.
[31] K. Nomura, Y. Ujihira, T. Hayakawa, K. Takehira, Appl. Catal. A 137 (1996) 25–36.
[32] K.M. Merz, J. Am. Chem. Soc. 112 (1990) 7973–7980.
[33] K.I. Peterson, W.J. Klemperer, Chem. Phys. 80 (1984) 2439–2445.
[34] M. Primet, P. Pichat, M.V. Mathieu, J. Phys. Chem. 75 (1971) 1220–1221.
[35] K. Tanaka, J.M. White, J. Phys. Chem. 86 (1982) 4708–4714.
[36] M.A. Henderson, Surf. Sci. 400 (1998) 203–219.
[37] S. Noirault, S. Celerier, O. Joubert, M.T. Caldes, Y. Piffard, Solid State Ionics 178 (2007) 1353–1359.
[38] R.A. Evarestov, A.V. Bandura, V.E. Alexandrov, Surf. Sci. 601 (2007) 1844–1856.
[39] R. Zhang, H. Alamdari, S. Kakiaguine, Appl. Catal. B 72 (2007) 331–341.
[40] A. Lindholm, N.W. Currier, E. Fridell, A. Yezerets, L. Olsson, Appl. Catal. B 75 (2007) 78–87.
[41] F. Grillo, M.M. Natile, A. Glisenti, Appl. Catal. B 48 (2004) 267–274.
[42] M.J. Scholten, J. Schoonman, J.C. Miltenburg, H.A.J. Oonk, Solid State Ionics 61 (1993) 83–91.
[43] B.V. L'vov, V.L. Ugolkov, Thermochim. Acta 409 (2004) 13–18.